ANNEALING EFFECT ON THE DEVELOPMENT OF KESTERITE STRUCTURE IN COPPER-ZINC-TIN SULFIDE (CZTS) THIN FILM

Utku CANCİ MATUR[1,2*]

[1]İstanbul Gedik Üniversitesi, Gedik MYO, Mekatronik Programı, İstanbul, TÜRKİYE
[2]İstanbul Gedik Üniversitesi Enerji Teknolojileri Uygulama ve Araştırma Merkezi, İstanbul, 34913, TÜRKİYE
ORCID No : http://orcid.org/0000-0001-6342-5645

Keywords

CZTS 1
Thin Films 2
Semiconductor 3
Optical Properties 4
Sol-Gel 5

Abstract

Copper-zinc-tin sulfide (Cu_2ZnSnS_4 or CZTS) is a p-type semiconductor material with a high absorption coefficient and an optimal energy band gap. It belongs to a quaternary semiconducting group of I2-II-IV-VI4. Economically and eco-friendly CZTS material is a good absorber layer for solar cells. In this study, CZTS thin films were coated on soda-lime silicate glass (SLSG) using the sol-gel dip-coating method at room temperature. CZTS thin films were annealed in an ambient atmosphere in an oven. X-ray diffraction (XRD) and scanning electron microscopy (SEM) were used to analyze structural properties, while optical properties were studied by UV-visible spectroscopy (UV–vis) and photoluminescence (PL). Elemental composition was determined by using energy-dispersive X-ray analysis (EDAX). Density functional theory calculations were performed using the HSE06 hybrid method, with the theoretical band gap closely matching the experimental value with a 9% difference. The XRD results indicated that annealing the thin films in an ambient atmosphere at high temperatures led to oxidation and deterioration of the kesterite CZTS form. The optical analysis shows that the energy band gap of the CZTS thin films (1.63 eV) matched the literature.

BAKIR-ÇİNKO-KALAY SÜLFÜR (CZTS) İNCE FİLMİNDE KESTERİT YAPISININ GELİŞİMİ ÜZERİNDE TAVLAMANIN ETKİSİ

Anahtar Kelimeler

CZTS 1
İnce Filmler 2
Yarı İletken 3
Optik Özellikler 4
Sol-Jel 5

Öz

Bakır-çinko-kalay sülfür (Cu2ZnSnS4 veya CZTS), yüksek soğurma katsayısına ve optimum enerji bant aralığına sahip p tipi bir yarı iletken malzemedir. I2-II-IV-VI4 kuaterner yarı iletken grubuna aittir. Ekonomik ve çevre dostu CZTS malzemesi güneş hücreleri için iyi bir soğurucu tabakadır. Bu çalışmada, oda sıcaklığında sol-jel daldırma kaplama yöntemi kullanılarak soda-kireç silikat cam (SLSG) üzerine kaplanmış CZTS ince filmleri. CZTS ince filmleri bir fırında ortam atmosferinde tavlanmıştır. Yapısal özellikleri analiz etmek için X-ışını kırınımı (XRD) ve taramalı elektron mikroskobu (SEM) kullanılırken, optik davranış UV-görünür spektroskopisi (UV-vis) ve fotolüminesans (PL) ile incelenmiştir. Elementel bileşim, enerji dağılımlı X-ışını analizi (EDAX) kullanılarak çıkarılmıştır. Yoğunluk fonksiyonel teorisi hesaplamaları, teorik bant aralığının deneysel değere %9 farkla yakın bir şekilde uyduğu HSE06 hibrit yöntemi kullanılarak gerçekleştirilmiştir. XRD sonuçları, ince filmlerin yüksek sıcaklıklarda ortam atmosferinde tavlanmasının kesterit CZTS formunun oksidasyonuna ve bozulmasına yol açtığını göstermiştir. Optik analiz, CZTS ince filmlerinin enerji bant aralığının (1,63 eV) literatürdeki verilerle uyumlu olduğunu göstermektedir.

Araştırma Makalesi		Research Article	
Başvuru Tarihi	: 16.09.2025	Submission Date	: 16.09.2026
Kabul Tarihi	: 03.04.2026	Accepted Date	: 03.04.2026

* Sorumlu yazar: utku.canci@gedik.edu.tr
https://doi.org/10.31796/ogummf.1785089

1. Introduction

The development of technology, the rapid increase in industrialization, and population have accelerated the increase in energy demand. Due to the energy crisis, researchers are searching for new solutions and developing new technologies. The risk of depletion of fossil fuels, which currently meet most of the energy demand, has negative effects on the environment, making it unfavorable for users. On the other hand, environmentally friendly, renewable energy sources such as solar energy, which don't have depletion risk, have gained popularity among researchers.

The photovoltaic effect follows a physical process that converts solar radiation into electricity. The materials such as Cadmium Telluride (CdTe), Copper-Indium-Sulphide (CIS), and Copper Indium Gallium selenide (CIGS), which are frequently used in photovoltaic technology fields, have been reported to reach efficiency values of 19.6%, 22.1%, and 23.35%, respectively (Baid et al. 2021). However, the fact that the elemental components of some of these materials are expensive or toxic has led researchers to study materials such as Copper-Zinc-Tin-Sulphide (CZTS), which is low-cost, abundant on earth, and environmentally friendly, with high photovoltaic efficiency (Li et al., 2016; Walsh, Che, We ve Gong, 2012; Zeng et al., 2014).

CZTS and CZTSe are p-type semiconducting compounds of I2-II-IV-VI4 with an optimal energy band gap and high absorption coefficient. Band gap tunability, electrical conductivity, and optical absorption properties are decisive for the performance of CZTS thin films in photovoltaic devices. CZT(S,Se) thin films' energy band gap is between 1.4 and 1.6 eV (Seboui, Gassoumi, Cuminal ve Turki, 2015; Tanaka, Moritake, Oonuki ve Uchiki, 2008) with low cost and high energy conversion efficiency. The highest photo-to-electric conversion efficiency (η) of CZTS thin-film solar cells values reported so far for pure sulfur Cu2ZnSnS4 (CZTS) is increasing from 9.2% (Zhang, You, Dan, Wan ve Dong, 2023; Sun et al., 2016) to 13% (Wei et al., 2023) while the predicted theoretical conversion efficiency is 31 % (Yussuf, Nwambaekwe, Ramorok ve Iwuoha, 2023). The electrical conversion efficiency of solar cells that used pure selenide $Cu_2ZnSnSe_4$ and mixed sulfa-selenide CZTSSe solar cells was 11.6 (Lee et al., 2015), and 12.6% (Wang et al., 2014), respectively. Many studies have been carried out to increase the efficiency of CZT(S, Se) solar cells, especially in improving the absorber (Haass et al., 2015; Kim, Kim, Tampo, Shibata ve Niki, 2016; Sun et al., 2017) and buffer layers (Han et al., 2016; Salim et al., 2016; Tao et al., 2016). Other functional layers of CZT (S, Se) solar cells are attempted to be produced by improving the interface qualities between the layers (Wei et al., 2018). For this reason, CZT (S, Se) thin films are more attractive than solar cells such as CIGS and GaAs (Cabas-Vidani, et al. 2018; Lafond et al., 2017). Vacuum and sputter-based methods, which are the most commonly used methods for the production of CZT (S, Se) thin film solar cells, are both expensive and complex techniques, as well as having low electrical conversion efficiencies. On the other hand, non-vacuum and solution-based production methods are cheap, highly efficient, and easy to implement (Katırcı et al., 2023).

In this study, CZTS thin film is deposited on substrates using the sol-gel dip coating method. Sol-gel method is low-cost, easy to implement, and influential. Also, the chemical composition can be adjusted as desired, and sub-micron-sized powders can be produced under low-temperature conditions. Crystalline features (in XRD analysis), the surface morphology (in SEM micrographs), and elemental composition were extracted by EDAX, exhibiting structural features detaily. The optical properties have indicated the practical development of CZTS thin film for photovoltaic applications. The theoretical investigation is based on the crystal structure obtained from XRD peaks. In addition, density functional theory (DFT) in the HSE06 scheme brings out the electronic properties, in particular, band structure and band gap. This study aims to produce CZTS thin films under optimal conditions by comparing experimental measurements with theoretical values for application in photovoltaic technology.

2. Experimental

Copper Chloride Dihydrate ($CuCl2{\cdot}2H_2O$), Zinc Chloride Dihydrate ($ZnCl_2{\cdot}2H_2O$), and Tin Chloride Dihydrate ($SnCl_2{\cdot}2H_2O$) were used, while ethanol (1/3) and deionized water (2/3) were mixed and used as a solvent. In addition, diethanolamine (DEA) will be used as a pH stabilizer, and thiourea ($SC(NH_2)_2$) will be added as a sulfur source. As a result, a transparent yellow sol-gel solution will be obtained. The elemental ratio of starting materials Cu, Zn, Sn, and S was used in a 2:1:1:8 ratio for the deposition of CZTS thin films by the sol-gel dip coating method.
The chemical formation of the CZTS specified elemental ratio of 2:1:1:8, is represented as:

$$2CuCl_2.2H_2O + ZnCl_2.2H_2O + SnCl_2.2H_2O + 8SC(NH_2)_2 + heat \rightarrow Cu_2ZnSnS_4 + byproducts \quad (1)$$

In the final CZTS film, the Chlorine (Cl) and the organic components of the Thiourea and DEA are decomposed and evaporated as volatile byproducts (such as HCl, CO_2, and N_2) during the drying and sulfurization steps. This method aimed to obtain the CZTS solution without requiring an extra sulfurization process. CZTS thin films were deposited on SLSG substrates by a sol-gel dip-coating technique using a dip coater. The substrates

were withdrawn at a rate of 200 mm/min. Then the substrates were placed in the solution for 5 seconds by utilizing the computer-controlled dip coater. The thickness of the films was measured by a surface profilometer, which is ~1000 nm for 10 layers. Figure 1 exhibits the solution form and the dip-coating process of the CZTS thin films. In this study, research and publication ethics were compiled with.

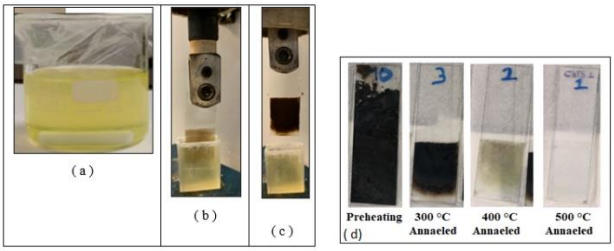

Figure 1(a-d): (a) The synthesized solution and the dip coating process of the CZTS thin films (b) after 5 layers (c) and after 10 layers, (d) Pre-heated and annealed CZTS thin film samples with 10 layers.

3. Results and discussion

3.1Structural properties of CZTS thin films

CZTS thin films were grown by the sol-gel dip coating method on SLG substrates by coating 10 layers. After each dipping, the substrates were pre-heated at 300°C for 5 minutes in an oven (air condition).

In this study, we examined the properties of the annealed CZTS thin films at different temperatures. The structural properties of the CZTS thin films were measured by using X-ray diffraction analysis (by the Shimadzu-6000 diffractometer with a Cu Kα (λ = 1.54 Å), radiation source Kα (λ = 1.54 Å). Scherrer relation was used to calculate the crystallite sizes (D). The D values of the peaks are shown in Table 1.1. The lattice constants "a" and "c" were estimated to be 5.41 Aº and 10.82 Aº, respectively. The lattice parameter values were almost the same as the standard values from JCPDS Card No. 26-0575 [20], which were a = 5.435 Aº and c = 10.843 Aº. Figure 2 exhibits the XRD of the sol-gel dip-coated CZTS thin films annealed at 500 °C for 45 minutes.

Figure 3 exhibits the XRD diffractometers of the sol-gel dip-coated CZTS thin films annealed at 400°C for 45 minutes. Figure 4 exhibits the XRD diffractometers of the sol-gel dip-coated CZTS thin films annealed at 300 °C for 45 minutes. The XRD patterns of the films annealed in an oven at 400°C and 500°C did not accurately represent the exact CZTS crystal structure due to oxidation. It was assumed that the crystal structure was slightly deteriorated as sulfur (S) became more volatile during the annealing process at 500°C, causing stoichiometry disorders in the structure.The XRD diffractometers exhibit Tin Sulfide (SnS) peaks annealed at 500°C and Zinc Sulfide (ZnS) peaks for the 400°C. However, the films annealed at 300 °C were shown XRD diffractometers peaks located at 2θ values 17.389°, 28.553°, 33.091°, 47.452° and 56.173° which correspond to the (101), (112), (200), (220), (312) and (332) planes respectively, of the kesterite tetragonal phase of CZTS. These results exhibit that the annealing temperature and annealing conditions were significant for the structural form of the CZTS thin film.

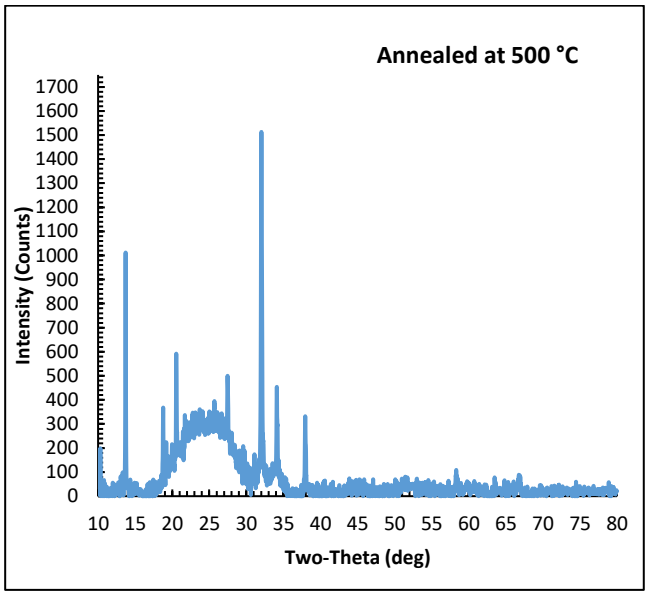

Figure 2: XRD of CZTS thin film annealed at 500 °C

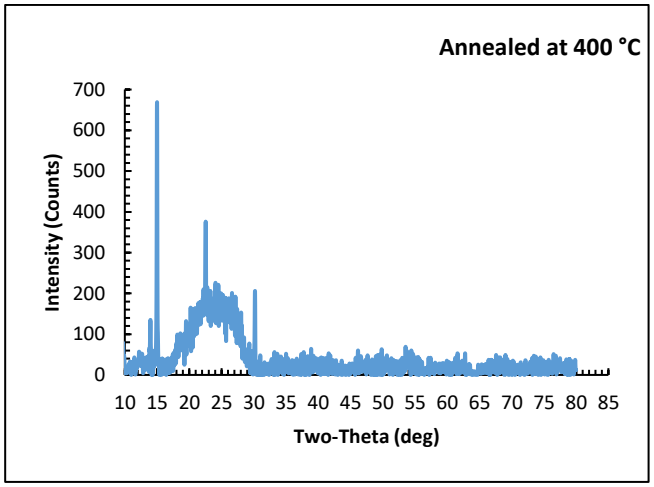

Figure 3: XRD of CZTS thin film annealed at 400 °C

This study provided detailed information about the diffraction peaks' widths, intensities, and locations. The XRD patterns of the CZTS thin film demonstrated the ability to differentiate between the kesterite and stannite phases based on their distinctive peaks and locations within the XRD pattern (see Fig. 4). This is because kesterite and stannite phases have distinct diffraction peaks due to their different crystal structures. The most intense peak has appeared at ~28-

32˚ for kesterite. It was determined that the kesterite peak has had a broader range between ~28-32˚. However, stannite has appeared above 32˚ (at ~33˚C with less intensity compared to kesterite in the sol-gel derived CZTS thin films). CZTS Thin Film annealed at 400 ˚C indicates that the crystal irregularities in the thin film have been largely eliminated. The CZTS thin film annealed at 400 ˚C, the atoms were prevented from being placed in different positions, and the crystal structure was ensured to be in an ideal kesterite arrangement.

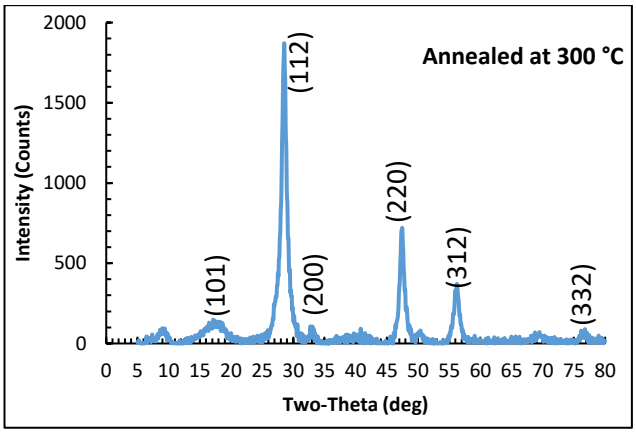

Figure 4: XRD of CZTS thin film annealed at 300 °C

In this study, by preventing the formation of a non-ideal crystal structure (such as stannite) in the CZTS thin film annealed at 300 °C, the recombination rate of carriers in the developed p-type semiconductor was modified. The XRD parameters of the CZTS thin films annealed at 300 °C are exhibited in Table 1.

Table 1: The XRD parameters of the CZTS thin film annealed at 300 °C in normal ambient

Film Sample	2θ	d value (A°)	FWHM (β)	D (nm)	Microstrain (ε) x10^{-3}
101	17.38	5.093	0.607	12.67	17.32
112	28.55	3.122	0.647	13.39	11.09
200	33.09	2.703	0.328	25.27	4.82
220	47.45	1.913	0.648	13.39	6.43
312	56.17	1.635	0.805	11.19	6.58
332	76.63	1.241	0.604	16.76	3.34

This study is carried out on CZTS nanostructures by the Williamson-Hall (W-H) method based on uniform deformation (UD). The CZTS thin film's crystallite size was measured by the Scherrer equation and Williamson–Hall plot, respectively. The influence of strain on the Bragg reflection's (hkl) line broadening is given by $\beta\varepsilon=4\varepsilon\tan\theta_{hkl}$, where ε is the microstrain and βτ is the broadening of the line caused by the crystallite size. Figure 5 displays W-H graphs of CZTS nanostructures via UD models. Using the formula c= Kλ/D (Mahewar, Vidule ve Ravangave, 2020), the average crystallite size is determined to be 13.21 nm, as illustrated in Figure 5.

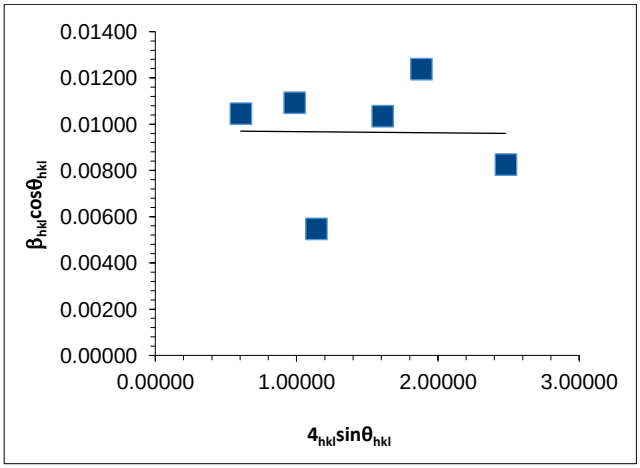

Figure 5: W-H graphs of CZTS nanostructures annealed at 300 °C

Figure 6 exhibits the SEM of sol-gel dip-coated CZTS thin films annealed at 300 °C. Some small grain sizes appear in the annealed films, which may be the Cu, Sn, and Zn phases according to the XRD spectra. During the annealing temperature at 300 °C, the CZTS formation reaction process was uniform, and only very small holes were observed at the film surface. However, at 580 °C sulfurization temperature in an N_2 environment, massive crystalline grains were seen without any holes or cracks (Udayabhaskar ve Karthikeyan, 2014).

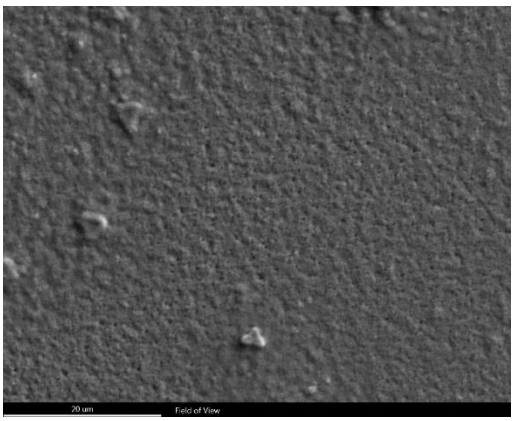

Figure 6: SEM of sol-gel dip-coated CZTS thin films annealed at 300 °C.

The EDAX spectra of annealed CZTSe thin films at 300 °C are displayed in Figure 7. Cu, Zn, Sn, and S have melting points of around 1085 °C, 419.5 °C, 231.9 °C, and 115.21 °C. The strong signals Cu, Zn, Sn, and S continents for the

creation of CZTS films are displayed in the EDAX pattern. The annealing temperature of 300 °C represents a critical threshold where the nucleation of the kesterite phase begins. At this temperature, the atomic mobility (diffusion) increases, allowing Cu, Zn, and Sn atoms to react with sulfur and initiate the formation of the lattice structure. However, if the temperature remains too low, the amorphous structure tends to be dominant; conversely, if the temperature is excessively high, it may lead to the formation of secondary phases such as ZnS and Cu2S. Table 2 exhibits the weight%, atomic%, and net intensity of the CZTS thin film. Figure 7 and Table 2 were matched with each other.

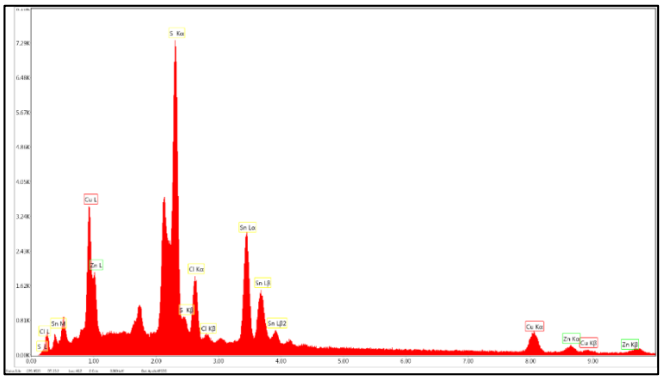

Figure 7: EDAX spectra of CZTS thin films annealed at 300°

Table 2. Weight (%), atomic (%), and net intensity of the CZTS thin film.

Element	Weight (%)	Atomic (%)	Net Int.	Error (%)
S K	31.49	51.68	1848.63	0
ClK	6.21	9.21	288.91	0.02
SnL	31.9	14.14	554.72	0.02
CuK	21.33	17.67	142.86	0.03
ZnK	9.07	7.3	44.74	0.05

The CZTS thin films were deposited by the sol-gel dip coating method, and all the films were pre-heated at 300 °C for each layer. The optical and structural properties of the CZTS thin films were analyzed by exposing them to different annealing temperatures. The results exhibit that annealing in normal ambient oxidizes the films, while we were exposed to annealing at 300 °C improved the crystal size, grain growth, and lowered the Sn-loss, ZnS, and carbon content for the CZTS thin films (Liu, et al., 2016; Aydoğmuş, 2024).

In this study, the reduction of chemical waste was provided for the fabrication of CZTS thin film using the sol-gel method. Thus, the amount of waste was reduced by using fewer chemicals compared to other production methods. As it was carried out at low annealing temperatures by using the sol-gel method, energy consumption was reduced, and the environmental impacts of the production process were decreased. As the used chemicals (during synthesis) were utilized more effectively in the sol-gel dip coating method, the waste of raw materials was reduced.

3.2. Optical properties of CZTS thin films

The diffuse reflectances of CZTS thin films, both annealed and unannealed, were measured between 300–1100 nm. The band-gap measurements can be determined via UV–vis–NIR techinique optically. The energy band gaps of the thin films were determined by the Tauc method et al. (Matur, Duru ve Akcan, 2022). The Tauc plot linear section was produced by applying the modified Tauc relation, which is provided by extrapolation to determine the optical band gap of the CZTS thin films.

$$\alpha h\nu = A\left(h\nu - E_g\right)^{\frac{1}{2}} \qquad (2)$$

where Eg is the bandgap energy and A is a constant. Plotting a graph of $(ahn)^2$ as a function of photon energy hu is necessary to calculate Eg. Given the energy band values of thin films, the linear portion of the graph is displayed with an intercept on the hn-axis. Figure 8-9 exhibits the energy band gap of the CZTS thin film annealed at 300 °C and 400 °C. The calculated band gap energy of the CZTS thin film annealed at 400 °C is 2.8 eV, 300 °C is 1.64 eV. The energy band gap of the films was matched with the PL of the films.

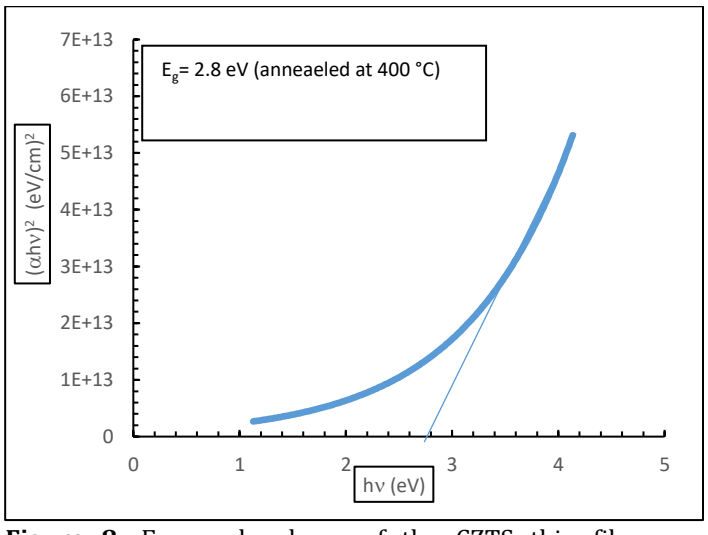

Figure 8: Energy band-gap of the CZTS thin film annealed at 400 °C

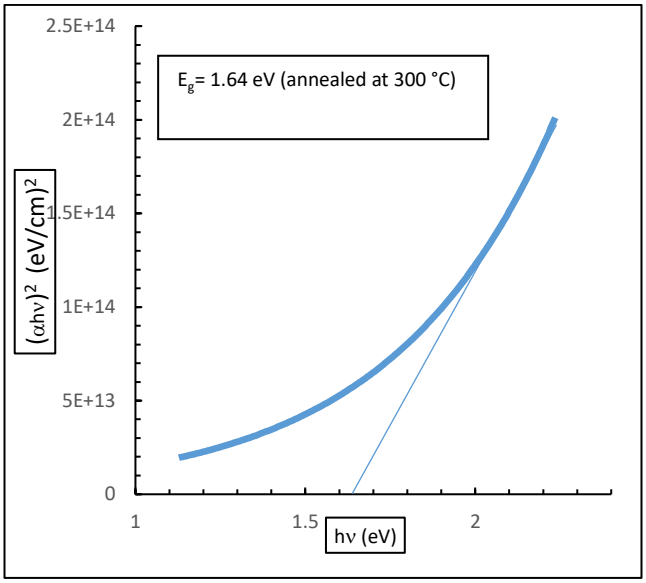

Figure 9: Energy band-gap of the CZTS thin film annealed at 300 °C

3.3. Photoluminescence and Crystal Defect Studies

The electronic structure of the CZTS thin films was analyzed with photoluminescence (PL) spectra. The transmittance of thin films were measured by the Shimadzu UV-mini 1240 spectrophotometer. Photoluminescence measurements were performed with Agilent -Varian Eclipse Fluorescence Spectrophotometer with excitation wavelength of 300 nm. The PL spectra of pre-heated CZTS thin films are shown in Figure 10.

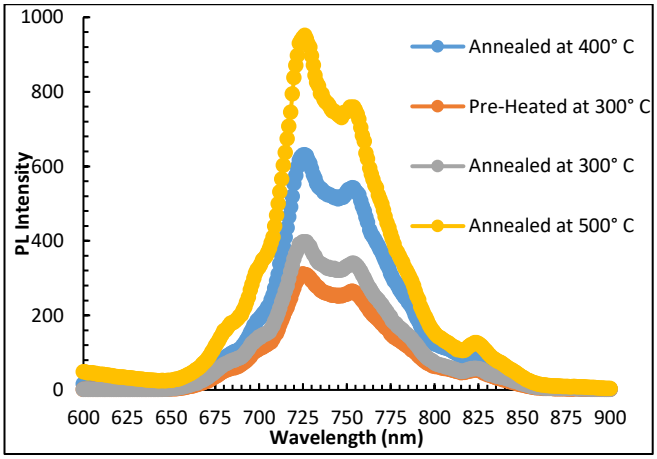

Figure 10: The PL spectra of the CZTS thin film

The film's PL spectra were captured by exciting the samples with the 395 nm radiation of the Hg lamp. Four important peaks are shown in Figure 10 in the range of 1.5 eV to 1.7 eV. The maximum intensity peak (1.7 eV) corresponded to the energy band gap of the CZT thin film, which was nearly matched with the optical measurements for annealing at 300°C. The PL intensity of the film increases with the increase of annealing temperature. The small shoulder around the 702 nm can be considered as ternary and quaternary alloys of CZTS. The higher peak at 728 nm can be associated with the formation of ternary alloys of CuZnS (Lakhe, Bhand, Londhe, Rohom ve Chaure, 2016).

3.4. First Principles Calculations

Density functional theory (DFT) provides a suitable perspective to reveal comparable results. It also allows for interconnecting the theory and experiment. This section concentrates on the structural and electrical properties of CZTS thin films theoretically. The CASTEP package is preferred for DFT calculations (Clark et al., 2005). The unit cell is constructed based on the lattice parameters, which are derived from the XRD peaks (a=b=5.41Å and c=10.82Å). Geometry optimization takes place shortly before ground state energy calculations, including the Koelling-Herman relativistic treatment. The LBFGS algorithm and HSE06 hybrid functional are applied, setting a cut-off energy of 800eV. The preferred SCF tolerance maximum displacement, maximum stress, and maximum force values are, respectively, 1.0×10-5eV/atom, 0.03eV/Å, 0.05GPa, and 0.001Å. In the HSE06 scheme, the norm-conserving pseudopotentials ensure the compatibility of hybrid functionals in usage. The computed unit cell is given in Figure 11. Besides, Table 3 presents the population and bond lengths of geometry-optimized atoms literally. To deal with the closest neighbors, the population analysis is performed up to a 3Å distance cut-off.

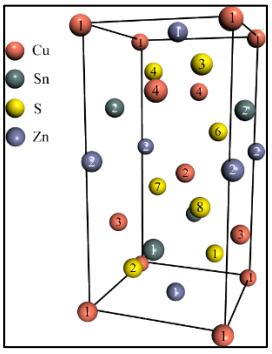

Figure 11: Geometry optimized unit cell of CZTS

The reddish, dark green, yellowish, and blueish spheres represent Cu, Sn, S, and Zn, respectively. The numerical labels are assigned to the atomic sites to fluently track the bond lengths given in Table 3. Distances up to 3Å are considered during population analysis. The distances between S-Cu, S-Zn, and S-Sn couples are given in Table 3. The significant part relies on the S-Sn bond lengths. The S-Sn closest bonds stay 2.35Å, 2.36Å, 2.37Å, 2.41Å, 2.42Å, and 2.46Å away from each other (2.39 in average). According to (Chuan-Jia et al., 2020), an increment in length leads the band gap decrease. In addition, the overall S-Sn bond population is barely higher than the rest.

Table 3: Bond lengths and population analysis

S -- Zn	Population	Length (Å)	S -- Sn	Population	Length (Å)
S7 -- Zn2	0.28	2.45	S2 -- Sn1	0.52	2.34
S6 -- Zn2	0.24	2.50	S1 -- Sn1	0.54	2.36
S4 -- Zn1	0.27	2.37	S7 -- Sn1	0.50	2.36
S3 -- Zn1	0.20	2.37	S6 -- Sn1	0.50	2.36
S1 -- Zn1	0.16	2.40	S3 -- Sn2	0.57	2.41
S5 -- Zn2	0.03	2.40	S5 -- Sn2	0.38	2.42
S2 -- Zn1	0.17	2.40	S4 -- Sn2	0.51	2.45
S -- Cu	**Population**	**Length (Å)**	**S -- Cu**	**Population**	**Length (Å)**
S7 -- Cu2	0.40	2.23	S7 -- Cu3	0.32	2.33
S3 -- Cu4	0.46	2.23	S1 -- Cu1	0.36	2.34
S4 -- Cu4	0.45	2.24	S1 -- Cu3	0.39	2.34
S6 -- Cu2	0.40	2.25	S4 -- Cu1	0.36	2.38
S5 -- Cu2	0.48	2.26	S2 -- Cu3	0.38	2.40
S5 -- Cu4	0.44	2.27	S6 -- Cu3	0.35	2.40
S3 -- Cu1	0.34	2.3	S2 -- Cu1	0.34	2.42

It was focused on the electronic states around the Fermi level to obtain the band-gap energy. The ground state and band structure calculations are carried out by the hybrid HSE06 functional. Cut-off energy, k-vectors, and SCF tolerance do not differ from the values used in geometry optimization. The band-gap energy (Eg) is calculated through the valance band maximum (VBM) and conduction band minimum (CBM). Note that, these are belong to the certain crystal momentum states, briefly k-vectors. The difference between VBM and CBM clearly gives the band-gap energy. When they lie through the same k-point, Eg has a direct band-gap character in which an electron can emit a photon directly.

Figure 12 shows the band-gap energies, VBM, and CBM; here with, the plot demonstrates the band-gap, and it is found to be 1.764 eV. In addition, the direct band-gap mechanism is in charge. The S-Sn bond length is the key controller of the band-gap energy (Park, Kim, Hood ve Walsh, 2018). The HSE06 funtional provides consistency with the experimentally calculated band gap (Chuan-Jia et al., 2020). Earlier theoretical investigations on band-gap engineering has estimated distinct values; moreover, relatively accurate approaches disagreed with the experimental findings. That may oftenly be related not only to the fabrication and measurement enviorenment but also theory-experiment mismatch under certain physical conditions Konan, 2023). However, the exact lattice parameters need to be derived following an experimental procedure, eg, XRD measurements indeed. Even though, the oxygen vacancies are not implemented to the unit cell, the resulted gap value is quite accurate. However, defects, exempli gratia, oxygen vacancies may affect the bond length of S-Sn.

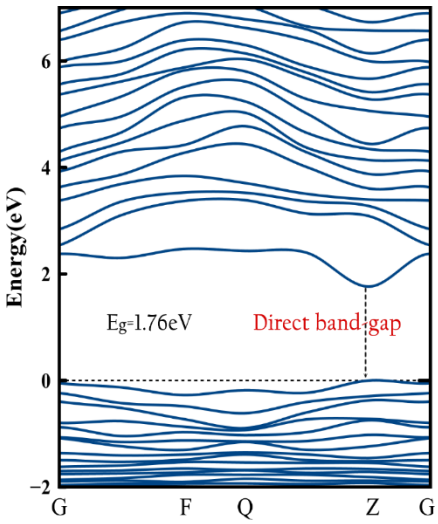

Figure 12: Band structure of geometry optimized CZTS by hybrid HSE06 functional: Unit cell is built on experimental lattice parameters

Deposition of CZTS thin film with a chalcogenide kesterite structure has provided several important technological advantages. Formation of the chalcogenide kesterite structure in CZTS thin film has enabled to growth of cost-effective thin films consisting of abundant and economical elements (Cu, Zn, Sn, S). Since the toxicity of the elements (Cu, Zn, Sn, S) used in the chalcogenide-kesterite structure is low, it has

enabled the creation of thin films that are safe for the environment and health.

Production of CZTS thin film using environmentally friendly solvents (ethanol and deionized water) has reduced the environmental impact of production processes. The high absorption coefficient created by ensuring that the In this study, by determining the production and optimization processes of CZTS thin film (including synthesis, coating process, post-coating process stages), the development of copper-zinc-tin sulfide thin film with high-efficiency potential and chalcogenide-kesterite structure was achieved.

4. Conclusion

In this study, annealed and unannealed CZTS thin films were compared structurally and optically to analyze the effect of these compounds on the appropriate energy band gap and the change of the optimum absorption coefficient (which was important for photovoltaic applications) was determined by examining the semiconductor properties of CZTS. The structural and optical properties have been determined (which was a significant step in the deposition of CZTS thin films) uniquely synthesized by the sol-gel method and their use in photovoltaic applications. By producing these thin films using the sol-gel dip coating method, it has been possible to precisely control the chemical composition in the film solution and optimize the thin film formation process most economically.

CZTS thin films are produced using the sol-gel dip coating method with a solution-based original receipt. CZTS thin films are exposed to pre-heating after each coating then at the end, some of them are annealed at different temperatures, such as 300°C, 400°C, and 500°C in air. According to the XRD analysis, increasing the annealing temperature in air decreases the crystallization. CZTS thin films annealed at low temperature (300°C) solely show better crystallization. However, increasing the temperature in the air should induce oxidation. The optical measurements indicate that the energy band gap is 1.63 eV for annealing at 300°C. The theoretical results strongly match the experimental findings when the HSE06 hybrid functional is preferred. The experimental conditions affect the physical properties of the structures, especially, S-Sn bond lengths and electronic band gap. Thus, the lattice parameters are implicitly comprised (for the samples annealed in air). It is concluded that producing CZTS thin film using an economically feasible and environmentally friendly sol-gel dip coating method at low temperatures is applicable to solar cell technology.

Acknowledgment

This work was supported by the Scientific Research Projects Coordination Unit of Istanbul Gedik University. Project name: ''Production of CZT(S,Se) Thin Film Solar Cells by Sol-Gel Dipping Technique''; Project number '' GDK202207- 15''.

Author Contributions

All authors contributed to the study conception and design. Material preparation, data collection and analysis were performed by Utku Canci Matur. The first draft of the manuscript was written by Utku Canci Matur commented on previous versions of the manuscript. All authors read and approved the final manuscript.

Conflict of Interest

The authors declare that they have no known competing financial interests or personal relationships that could have appeared to influence the work reported in this paper. Data availability will be made on reasonable request.

References

Aydoğmuş, Tuna. (2024). "Effect of temperature on oxidation during boriding of Ni-Hard 4" Materials Testing, vol. 66, no. 5, 2024, pp. 744-748. https://doi.org/10.1515/mt-2023-0385.

Baid, M., Hashmi, A., Jain, B., Singh, A. K., Susan, M. A. B. H., & Aleksandrova, M. (2021). A comprehensive review on Cu 2 ZnSnS 4 (CZTS) thin film for solar cell: forecast issues and future anticipation. Optical and Quantum Electronics (2021) 53:656 https://doi.org/10.1007/s11082-021-03272-5

Cabas-Vidani, A., Haass, S. G., Andres, C., Caballero, R., Figi, R., Schreiner, C., Bleiner, D. (2018). ''High-Efficiency (LixCu1− x)2ZnSn (S,Se)4 Kesterite Solar Cells with Lithium Alloying'', Advanced Energy Materials, 1801191.

Chuan-Jia Tong, Holly J. Edwards, Theodore D. C. Hobson, Ken Durose, Vinod R. Dhanak, Jonathan D. Major, and Keith P. McKenna, (2020). The Journal of Physical Chemistry Letters 2020 11 (24), 10463-10468 DOI: 10.1021/acs.jpclett.0c03205.

Clark SJ, Segall MD, Pickard CJ, Hasnip PJ, Probert MIJ, R Keith, CP Mike, (2005). First-principles methods using CASTEP. Zeitschrift fuer Kristallographie 220 (2005) 567-570.

Haass, S. G., Diethelm, M., Werner, M., Bissig, B., Romanyuk, Y. E., Tiwari, A. N. (2015). ''11.2% efficient solution processed kesterite solar cell with

a low voltage deficit'', Advanced Energy Materials, 5(18), 1500712.

Han, J., Jian, Y., He, Y., Liu, Y., Xiong, X., Cha, L., Schimper, H.-J. (2016). ''Nanostructures of CdS thin films prepared by various technologies for thin film solar cells'', Materials Letters, 177, 5-8.

Katırcı, R., Önel, M.N., Danacı, I., Danaci, I.K., Ozbay, S., Erden, F., (2023). Fabrication of CZTS films via combined electrodeposition and solution process: Experimental and first-principles study, ChemElectroChem 10 (2023) e202300162.

Kim, S., Kim, K. M., Tampo, H., Shibata, H., Niki, S. (2016). ''Improvement of voltage deficit of Ge-incorporated kesterite solar cell with 12.3% conversion efficiency'', Applied Physics Express, 9(10), 102301.

Konan, G. G. (2023). Spectroscopic Properties Including Line Strengths, Wavelengths, and Transition Probabilities for Hf LXII. Journal of Applied Spectroscopy, 90(4), 840-846. DOI 10.1007/s10812-023-01605-8.

Lafond, A., Guillot-Deudon, C., Vidal, J., Paris, M., La, C., Jobic, S. (2017). ''Substitution of Li for Cu in Cu2ZnSnS4: Toward wide band gap absorbers with low cation disorder for thin film solar cells'', Inorganic chemistry, 56(5), 2712-2721.

Lakhe, M. G., Bhand, G. R., Londhe, P. U., Rohom, A. B., & Chaure, N. B. (2016). Electrochemical synthesis and characterization of Cu2ZnSnS4 thin films. Journal of Material Science & Engineering, 5, 1000261.

Lee, Y. S., Gershon, T., Gunawan, O., Todorov, T. K., Gokmen, T., Virgus, Y., Guha, S. (2015). ''Cu2ZnSnSe4 thin-film solar cells by thermal co-evaporation with 11.6% efficiency and improved minority carrier diffusion length''. Advanced Energy Materials, 5(7), 1401372.

Li, J., Shen, H., Wang, W., Chen, J., Shang, H., Li, Y., Zhai, Z. (2016). Improvement of CZTSSe thin film solar cell by introducing a three-layer structure precursor. Materials Letters, 172, 90-93. https://doi.org/10.1016/j.matlet.2016.02.078

Liu, R., Tan, M., Zhang, X., Chen, J., Song, S., Zhang, W. (2016). Impact of sol-gel precursor treatment with preheating temperature on properties of Cu2ZnSnS4 thin film and its photovoltaic solar cell. J. Alloys Compd. 655, 124–129.

Mahewar, R. B., Vidule, R. R., & Ravangave, L. S. (2020). Structure, morphology and optical parameters of spray deposited CZTS thin films for solar cell applications. Indian J. Sci. Technol, 13(21), 2149-2156.

Matur, U. C., Duru, I. P., & Akcan, D. (2022). Tracking optical properties of ZnO: Mg thin films: Experimental and first principles calculations. Ceramics International, 48(13), 19090-19097.

Park, J.-S.; Kim, S.; Hood, S. N.; Walsh, A., (2018). Open-Circuit, Voltage Deficit in Cu2ZnSnS4 Solar Cells by Interface Bandgap, Narrowing. Appl. Phys. Lett. 2018, 113, 212103.

Salim, H., Olusola, O., Ojo, A., Urasov, K., Dergacheva, M., Dharmadasa, I. (2016). ''Electrodeposition and characterisation of CdS thin films using thiourea precursor for application in solar cells'', Journal of Materials Science: Materials in Electronics, 27(7), 6786-6799.

Seboui, Z., Gassoumi, A., Cuminal, Y., Turki, N. K. (2015). ''The post-growth effect on the properties of Cu2ZnSnS4 thin films'', Journal of Renewable and Sustainable Energy, 7(1), 011203.

Sun, K., Yan, C., Liu, F., Huang, J., Zhou, F., Stride, J. A., Hao, X. (2016). ''Over 9% efficient kesterite Cu2ZnSnS4 solar cell fabricated by using Zn1–xCdxS buffer layer'', Advanced Energy Materials, 6(12), 1600046. https://doi.org/10.1002/aenm.201600046.

Sun, R., Zhao, M., Zhuang, D., Gong, Q., Guo, L., Ouyang, L., Wei, Y. (2017). ''High-sulfur Cu2ZnSn(S, Se)4 films by sulfurizing as-deposited CZTSe film: The evolutions of phase, crystallinity and S/(S+ Se) ratio'', Journal of Alloys and Compounds, 695, 3139-3145.

Tanaka, K., Moritake, N., Oonuki, M., Uchiki, H. (2008). ''Pre-annealing of precursors of Cu2ZnSnS4 thin films prepared by sol–gel sulfurizing method'', Japanese Journal of Applied Physics, 47(1S), 598. https://doi.org/10.1063/1.4908063.

Tao, J., Liu, J., Chen, L., Cao, H., Meng, X., Zhang, Y., Chu, J. (2016). ''7.1% efficient co-electroplated Cu 2 ZnSnS 4 thin film solar cells with sputtered CdS buffer layers'', Green Chemistry, 18(2), 550-557.

Udayabhaskar, R., & Karthikeyan, B. (2014). Role of micro-strain and defects on band-gap, fluorescence in near white light emitting Sr doped ZnO nanorods. Journal of Applied Physics, 116(9).

Walsh, A., Chen, S., Wei, S. H., Gong, X. G. (2012). ''Kesterite thin-film solar cells: advances in materials modelling of Cu2ZnSnS4'', Advanced Energy

Materials,2(4),400-409. https://doi.org/10.1002/aenm.201100630

Wang, W., Winkler, M. T., Gunawan, O., Gokmen, T., Todorov, T. K., Zhu, Y., Mitzi, D. B. (2014). ''Device characteristics of CZTSSe thin-film solar cells with 12.6% efficiency'', Advanced Energy Materials, 4(7), 1301465.

Wei, H., Li, Y., Cui, C., Wang, X., Shao, Z., Pang, S., & Cui, G. (2023). Defect suppression for high-efficiency kesterite CZTSSe solar cells: advances and prospects. Chemical Engineering Journal, 462, 142121. https://doi.org/10.1016/j.cej.2023.142121.

Wei, Y., Zhuang, D., Zhao, M., Gong, Q., Sun, R., Zhang, L., Wu, Y. (2018). ''Effects of selenium atmosphere on grain growth for CZTSe absorbers fabricated by selenization of as-sputtered precursors'', Journal of Alloys and Compounds, 755, 224-230.

Yussuf, S.T., Nwambaekwe, K.C., Ramoroka, M.E., Iwuoha, E.I., (2023). Photovoltaic efficiencies of microwave and Cu2ZnSnS4 (CZTS) superstrate solar cells, Mater. Today Sustainability 21 100287, https://doi.org/10.1016/j.mtsust.2022.100287 (ISSN 2589–2347).

Zeng, X., Tai, K. F., Zhang, T., Ho, C. W. J., Chen, X., Huan, A., Wong, L. H. (2014). ''Cu2ZnSn(S, Se)4 kesterite solar cell with 5.1% efficiency using spray pyrolysis of aqueous precursor solution followed by selenization'', Solar Energy Materials and Solar Cells, 124,55-60. https://doi.org/10.1016/j.solmat.2014.01.029

Zhang, W., You, C., Dan, Z., Wang, W., & Dong, R. (2023, February). Improved performance of Cd-free CZTS thin-film solar cells by using CZTS0. 4Se0. 6 BSF layer. In Journal of Physics: Conference Series (Vol. 2418, No. 1, p. 012002). DOI 10.1088/1742-6596/2418/1/012002.